Supporting Information

Dendrite-Free Zn Anode Enabled by Anionic Surfactant-Induced Horizontal Growth for Highly-Stable Aqueous Zn-Ion Pouch Cells

Yuexing Lin, Zhaoxu Mai, HaiKuan Liang, Yan Li,

Gongzheng Yang, Chengxin Wang**

State Key Laboratory of Optoelectronic Materials and Technologies, School of Materials Science and Engineering, Sun Yat-sen (Zhongshan) University, Guangzhou 510275, People's Republic of China

**Correspondence and requests for materials should be addressed to C. X. Wang and G. Z. Yang.*

Tel & Fax: +86-20-84113901

E-mail: wchengx@mail.sysu.edu.cn; yanggzh5@mail.sysu.edu.cn.

Experimental section

Materials: Zinc sulfate heptahydrate ($ZnSO_4 \cdot 7H_2O$, 99.995%), SPS (90%), vanadium pentoxide (V_2O_5, 99.5%), and sodium sulfate (Na_2SO_4, 99.0%) were purchased from Sigma-Aldrich. Zn foils (100 μm thickness) and a glass fiber filter (Whatman, GF/D, 100 mm diameter) were used to assemble coin and pouch cells.

Electrolyte preparation: A 1 M $ZnSO_4$ aqueous electrolyte was prepared by dissolving 0.01 mol of $ZnSO_4 \cdot 7H_2O$ in deionized water, to obtain 10 mL of ZS solution at room temperature. Modified electrolytes were prepared by adding appropriate amounts of SPS to the 1 M $ZnSO_4$ electrolyte. For example, the 1 M $ZnSO_4$ electrolyte with 0.01 M SPS was prepared by dissolving 0.01 mol of $ZnSO_4 \cdot 7H_2O$ and 0.0001 mol of SPS in deionized water to obtain 10 mL of SPS 10 solution at room temperature. The 1 M $ZnSO_4$ electrolytes with 0.002 or 0.05 M SPS were prepared in the same way. The optimized concentration of SPS was 0.01 M.

Preparation of $V_2O_5 \cdot H_2O$ cathode material: The $V_2O_5 \cdot H_2O$ cathode material was prepared by reacting V_2O_5 powder and 30% H_2O_2 solution at room temperature. The reaction was similar to that reported in previous studies. [1, 2] V_2O_5 powder (1.092 g) and 4.8 mL 30% H_2O_2 were successively added to 60 mL deionized water and stirred at room temperature for 2 h. As the reaction proceeded, the color of the mixture gradually changed from yellowish-green to reddish-brown. After resting for 12 h, the $V_2O_5 \cdot H_2O$ precipitate was cleaned by washing three times with deionized water and ethanol in sequence and freeze-dried for 12 h.

Assembly of cells: Each coin-type Zn||Zn symmetrical cell consisted of two Zn foils of 12 mm diameter and a GF/D separator of 16 mm diameter. The added amount of electrolyte was ~ 80 μL. The Zn||Cu cells contained Zn foils of 12 mm diameter as anodes and copper foils of 14 mm diameter as cathodes. VOH cathodes were prepared

by a standard method: VOH was mixed with carbon black and polyvinylidene fluoride (PVDF) in a mass ratio of 7:2:1 and ground for 0.5 h. Then, the mixture was mixed with an appropriate amount of *N*-methyl-2-pyrrolidone (NMP) solvent and stirred to form a slurry. After that, the slurry was evenly spread onto graphite paper and dried at 80 ℃. The dried cathodes were cut into discs of 12 mm diameter, each carrying approximately 2.08 mg of VOH. The coin-type Zn||VOH full cells were assembled from the above cathodes and Zn anodes with a diameter of 14 mm. Each pouch-type symmetric cell consisted of two 3×5 cm^2 Zn foils as electrodes and a 4×6 cm^2 glass fiber separator. The shell of the pouch cell was an aluminum–plastic film and the amount of electrolyte was 2 mL. Similar materials were used for the pouch Zn||VOH full cells, except that 2.5×4.5 cm^2 VOH cathodes were used instead of the Zn foils on one side.

Material characterizations: SEM images were obtained using a Regulus 8230 instrument at 10 kV, and EDS mapping images were recorded at 10 kV. XRD patterns were obtained using a Rigaku diffractometer (Cu K_α radiation, λ = 0.154 nm). FT-IR data were collected using a Fourier transform infrared spectrometer (NICOLET 6700). Electrochemical AFM images were obtained with a Dimension Fastscan Bio instrument. A homemade device consisting of a PTFE electrolytic cell and two zinc foil electrodes was used in the measurements. During the test, the AFM probe was inserted into the electrolyte and placed in direct contact with the electrode surface. A much lower current was applied in the ZS electrolyte (0.1 mA cm^{-2}) than in the SPS10 electrolyte (1 mA cm^{-2}). Upon increasing the current to 0.5 mA cm^{-2}, Zn dendrites grew rapidly and the AFM test had to be stopped.

Electrochemical measurements: The Tafel, CV, EIS, CA, LSV, and overpotential curves were recorded using a DH7000 electrochemical workstation. Galvanostatic cycling and rate capability tests were conducted with a Neware testing system. Tafel

curves were measured from −0.25 to 0.25 V at a scan rate of 0.5 mV s^{-1}. CV curves were measured using Zn||Ti coin cells in a voltage range of −0.2 to 0.6 V at a scan rate of 5 mV/s. EIS data were obtained in the frequency range of 100 kHz to 0.1 Hz, at a voltage amplitude of 5 mV. CA tests were conducted using Zn||Zn symmetric cells under a bias voltage of −100 mV for 600 s. LSV curves were measued using Zn||Ti coin cells in a voltage window of −0.8 to −2.1 V at a scan rate of 5 mV s^{-1}. Nucleation overpotentials were measured at the current density of 1 mA cm^{-2} in Zn||Zn cells, and data points were collected every 0.1 s.

DFT calculations: DFT calculations were carried out using the Vienna Ab Initio Simulation Package (VASP).[3, 4] The Perdew–Burke–Ernzerhof functional[5, 6] was employed for calculating the exchange–correlation energy within the generalized gradient approximation,[7] and the projector augmented wave method[8, 9] was used to describe electron–ion interactions. The DFT-D3[10] approach was applied to take into account van der Waals (vdW) interactions. The plane-wave cutoff energy was set to 520 eV in all calculations. The Visual Molecular Dynamics (VMD) software was used to visualize structural data.[11, 12]

The SPS molecule was fully relaxed in a cubic box with a = 30 Å, as shown in Figure S1 (ESI). Slab models were used to construct periodic (002), (100), and (101) surfaces of Zn (Figure S15); the configurations of adsorbed SPS on these surfaces are shown in Figure 3c. The same supercell was employed for slabs with and without adsorbed SPS. The lattice parameters of the supercells were $a = b$ = 18.65 Å, $\alpha = \beta$ = 90° and γ = 120° for Zn (002), a = 16.65 Å, b = 19.79 Å and $\alpha = \beta = \gamma$ = 90° for Zn (100), and a = 16.86, b = 18.65, $\alpha = \beta$ = 90° and γ = 103.72° for Zn (101). The models of SPS@Zn(002), SPS@Zn(100), and SPS@Zn (101) contained 175, 196 and 154 atoms, respectively. Vacuum gaps larger than 20 Å were inserted between periodic slabs to eliminate their mutual interactions. To mimic the bulk structure of Zn, the bottom layers of the slab were fixed during the structural relaxation. A 1×1×1

Monkhorst–Pack (MP)[13] *k*-point mesh was applied for relaxing the nuclear degrees of freedom until the magnitude of the force acting on all atoms was less than 0.05 eV/Å. A 2×2×1 MP *k*-point mesh was employed for calculating the total energies of SPS@Zn systems, with an energy convergence threshold of 10^{-6} eV.

Adsorption energies were calculated as:

$$E_{ads} = E_{tot} - E_{slab} - E_{SPS}$$

where $E_{tot,}$ E_{slab}, and E_{SPS} are the total energies of the SPS@Zn system, the Zn slab, and the SPS molecule, respectively.

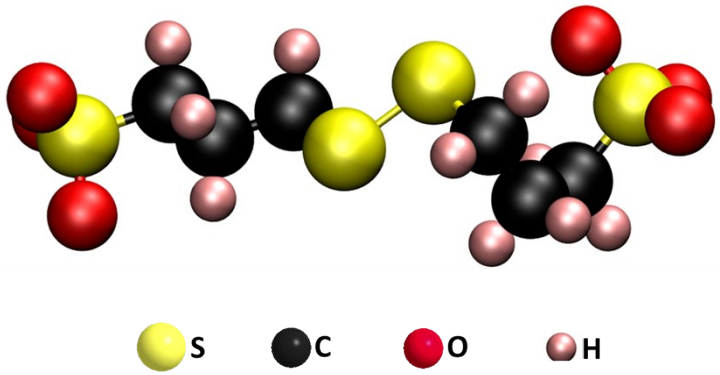

Figure S1. Fully relaxed configuration of SPS anion.

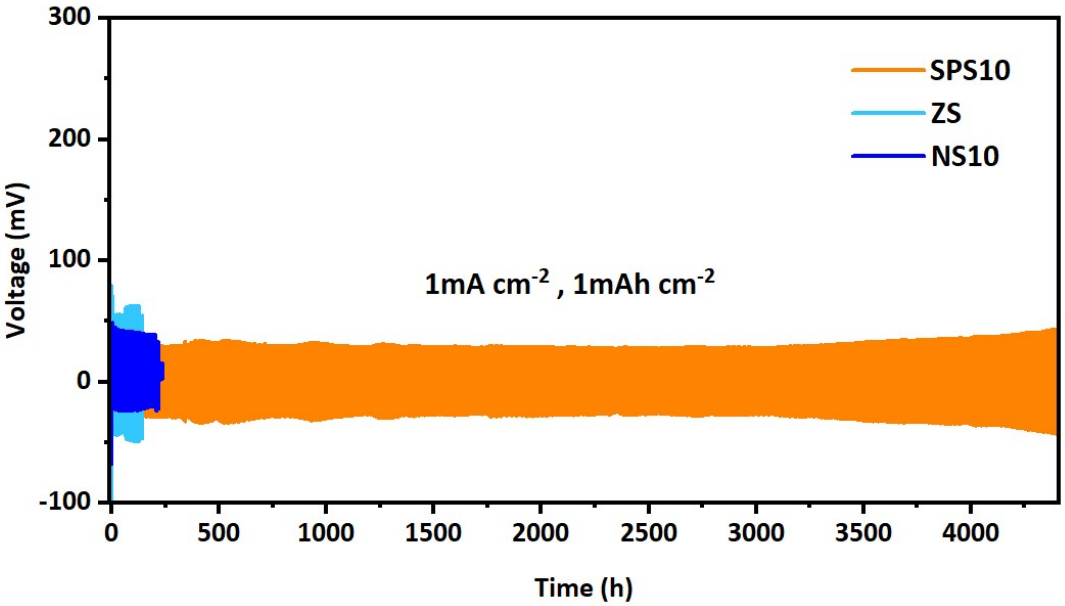

Figure S2. Galvanostatic Zn plating/stripping in Zn||Zn symmetric cells using $ZnSO_4$-based electrolytes with different additives.

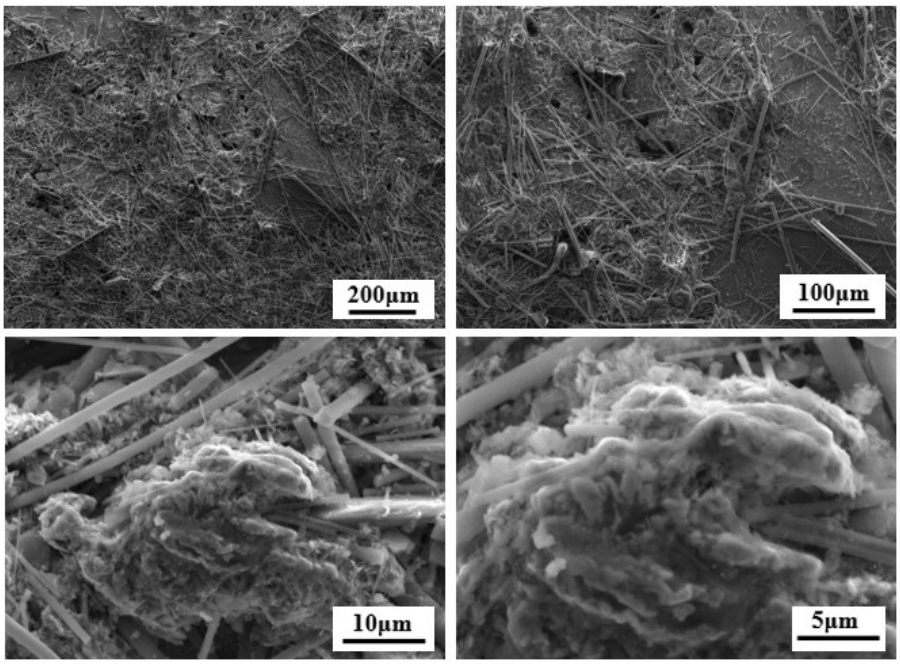

Figure S3. SEM images of Zn anode after 50 cycles at a current density of 1 mA cm^{-2} and a capacity density of 1 mAh cm^{-2} in symmetric cells using 1 M ZS + 0.01 M Na_2SO_4 electrolyte.

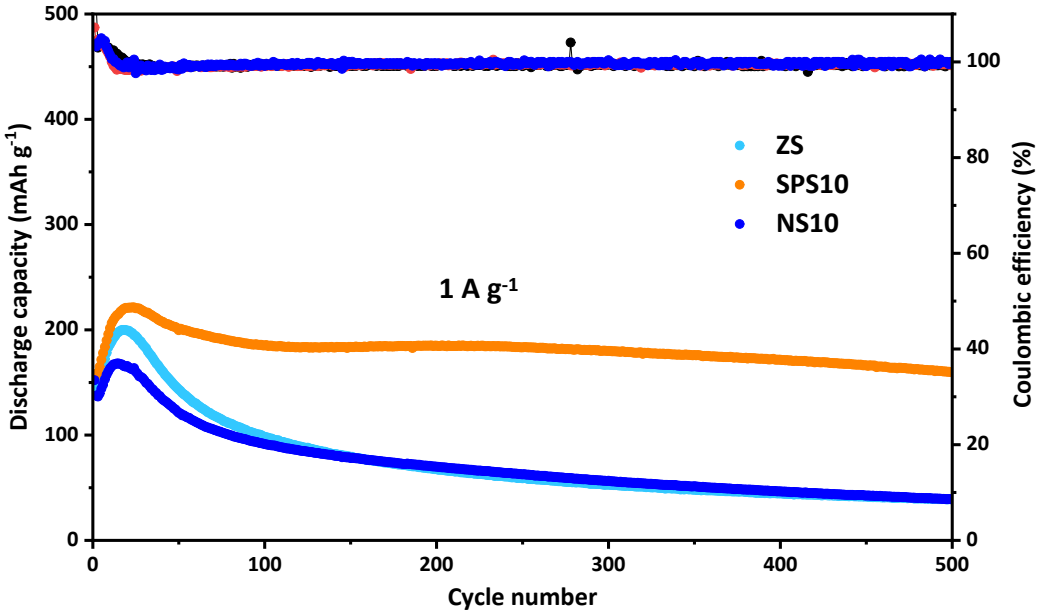

Figure S4. Long-term cycling performance of the Zn||VOH full cells at 1 A g^{-1} in different $ZnSO_4$-based electrolytes.

We replaced the 0.01 M SPS by 0.01 M sodium sulfate as electrolyte additive (the obtained electrolyte was denoted as NS10) and investigated the influence of sodium ions on the battery performances, and the results are shown in Figures S2-S4. As seen in Figure S2, the lifespan of the symmetric cell assembled using the NS10 electrolyte was only about 200 h, which is only slightly better than that using the ZS electrolyte and much poorer than that using the SPS10 electrolyte. The morphology of cycled anodes using the NS electrolyte was observed by SEM measurement. It was found that the morphology was similar to the anodes assembled using the ZS electrolyte (Figure S3). There were large amounts of dendrites and glass fibers on the anode surface. This suggests that the NS10 electrolyte was unable to regulate the homogeneous deposition of Zn. As presented in Figure S4, Zn||VOH full cell assembled using the NS10 electrolyte showed a capacity and cycling stability that were similar to those in the ZS electrolyte. In conclusion, the sodium ions cannot help to realize the uniform zinc deposition and improve the cycle stability of the full cell. Therefore, we speculate that it is the SPS anions that are responsible for modifying uniform zinc deposition.

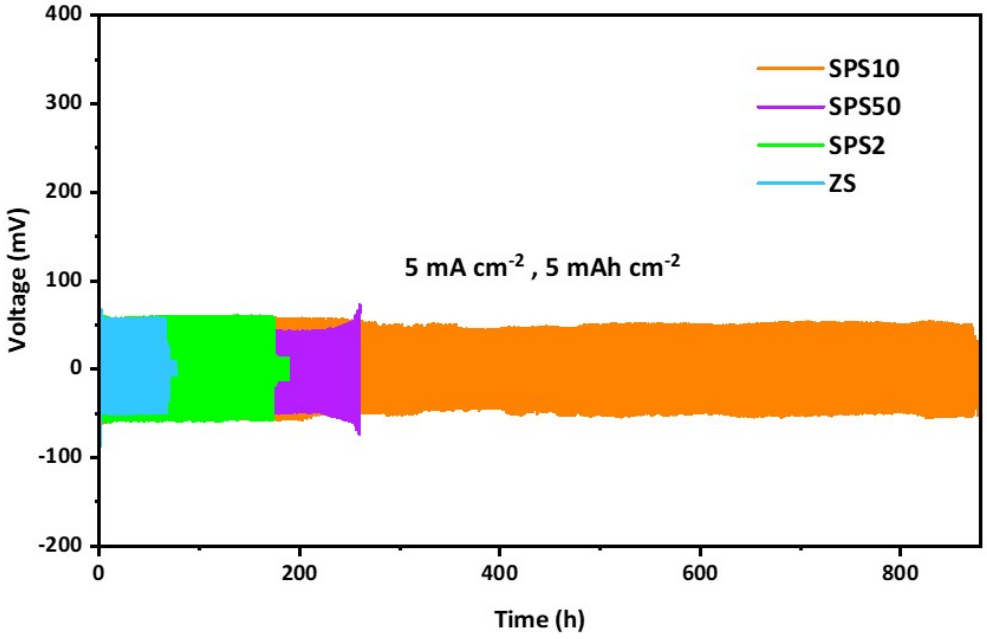

Figure S5. Galvanostatic cycling performance of Zn||Zn symmetric cells assembled using the electrolytes containing different concentrations of SPS.

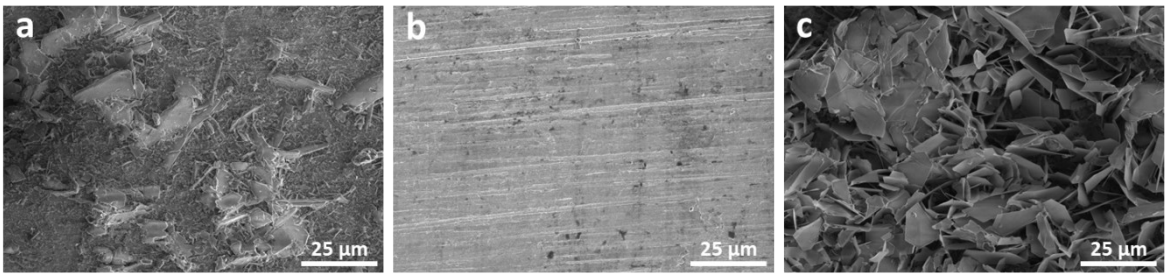

Figure S6. SEM images of bare Zn foil soaked in the a) SPS2, b) SPS10 and c) SPS50 electrolytes for 1 day.

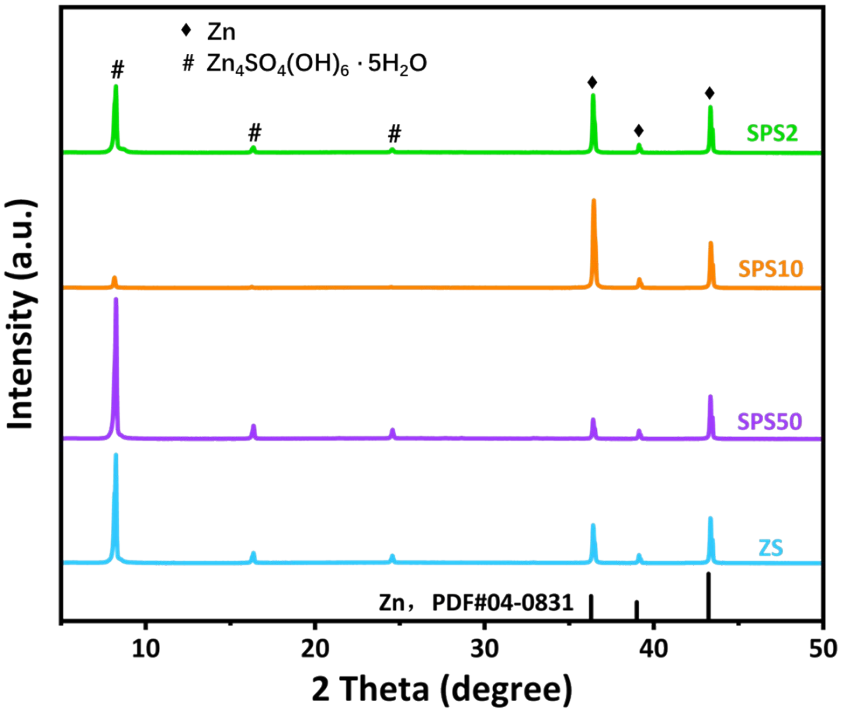

Figure S7. XRD patterns of the Zn foils soaked in the different electrolytes for 1 day.

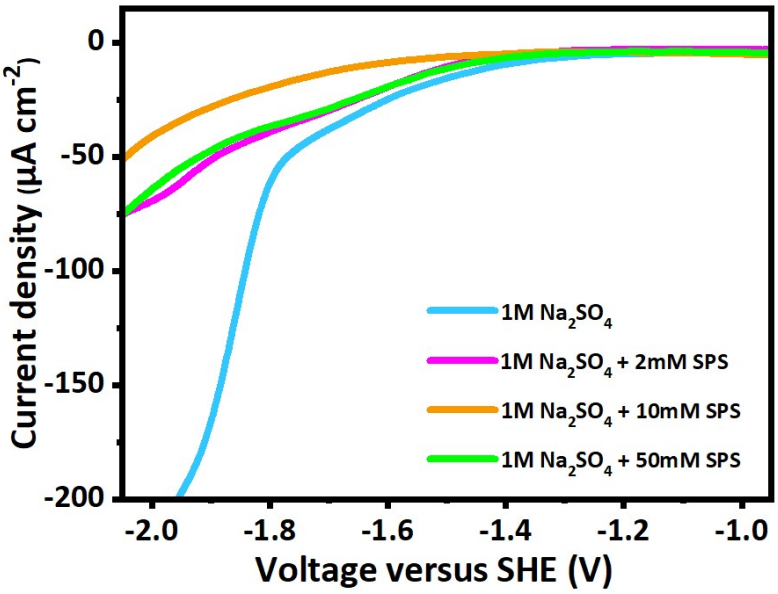

Figure S8. LSV test plot of Na_2SO_4 electrolyte containing different concentrations of SPS.

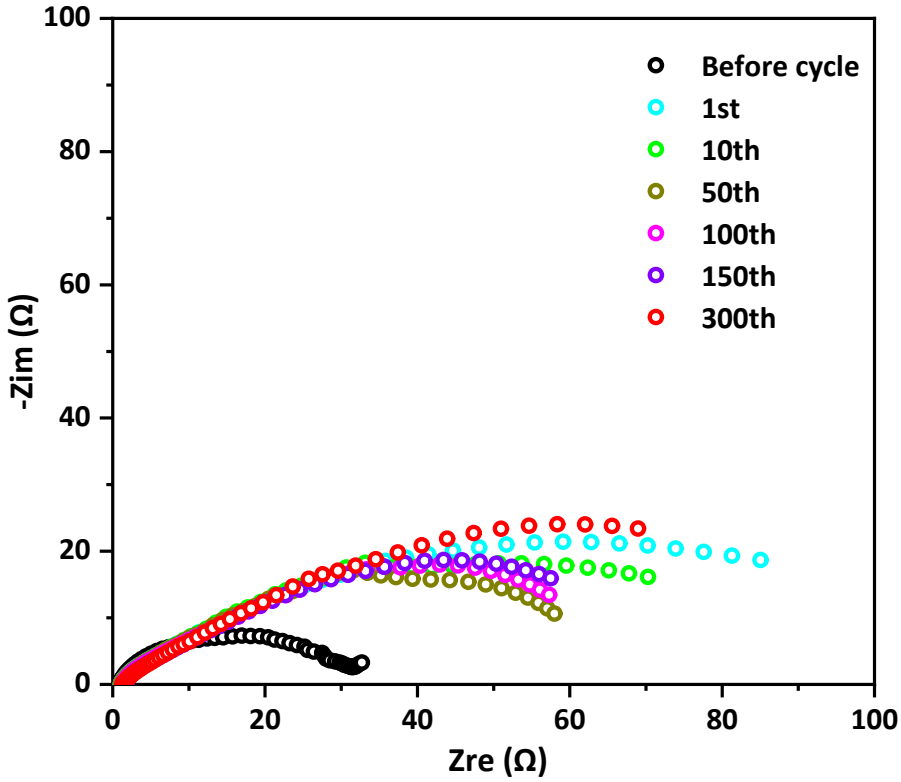

Figure S9. EIS plot of Zn||Zn symmetric cell assembled using the SPS10 electrolyte after different cycles.

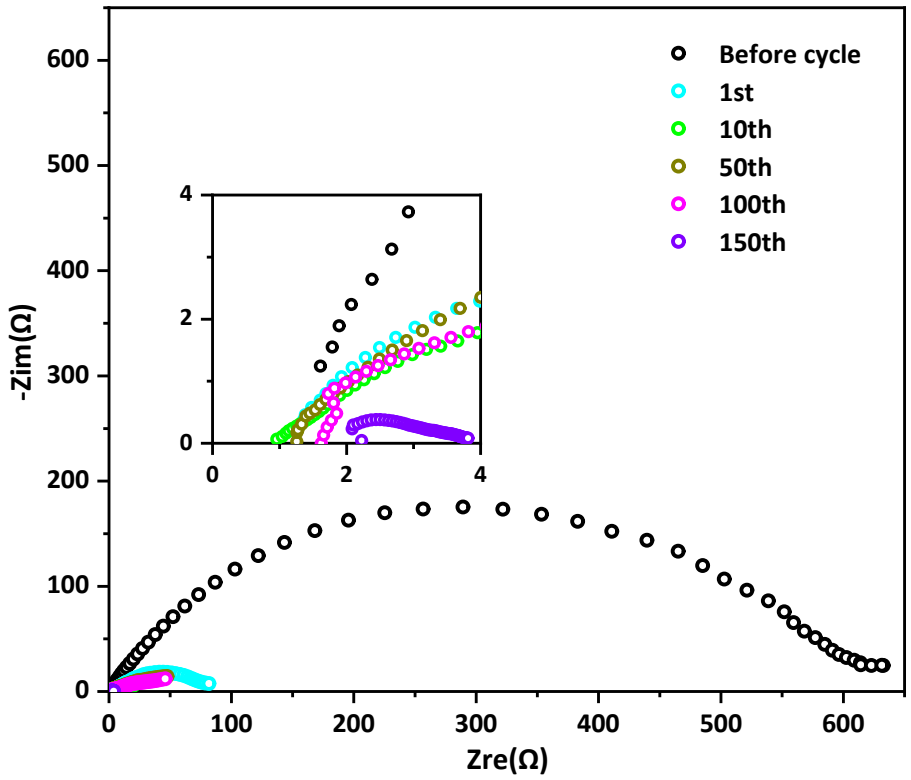

Figure S10. EIS plot of Zn||Zn symmetric cell assembled using the ZS electrolyte after different cycles. The inset shows the enlarged EIS diagram.

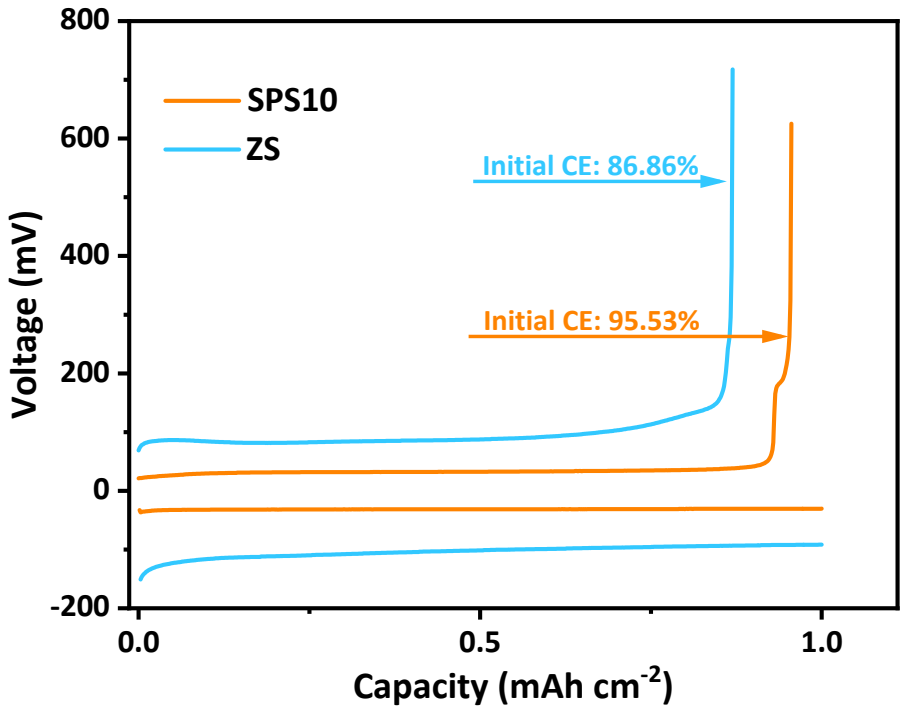

Figure S11. Voltage profiles of the first Zn plating/stripping cycle in Zn||Cu asymmetric cells assembled using different electrolytes.

Figure S12. The optical images of cycled Zn anodes after 50 cycles in different electrolytes (left: ZS; right: SPS10).

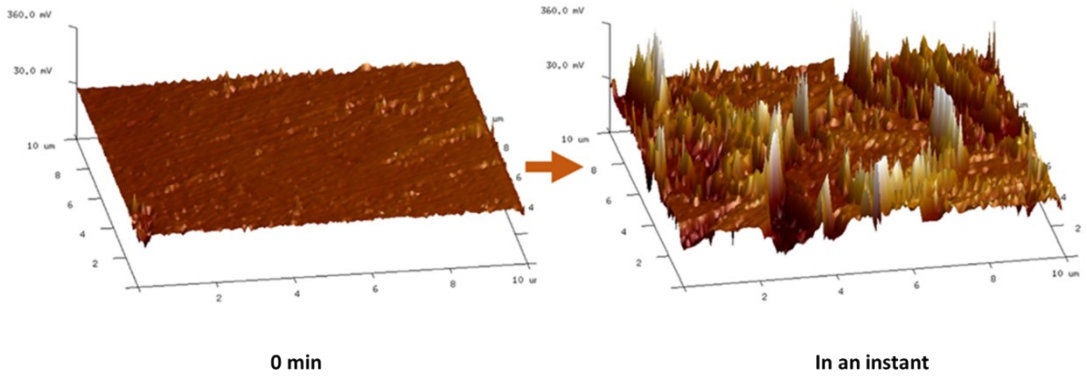

Figure S13. Images of Zn deposition in ZS electrolytes at large current observed by in situ AFM.

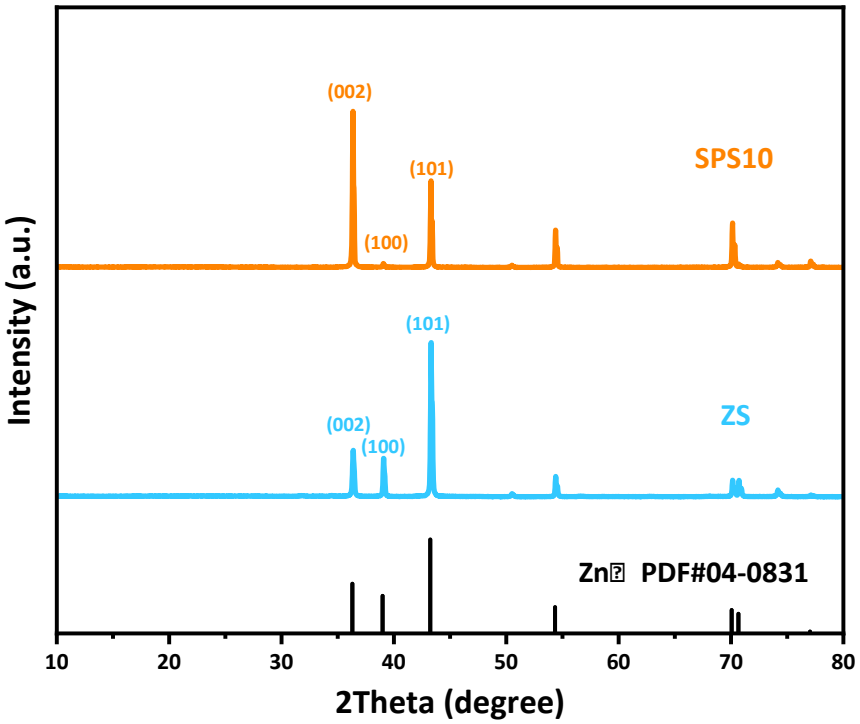

Figure S14. XRD patterns of electroplated Zn on Cu foils with a fixed capacity of 10 mAh cm^{-2} at a current density of 1 mA cm^{-2} in different electrolytes.

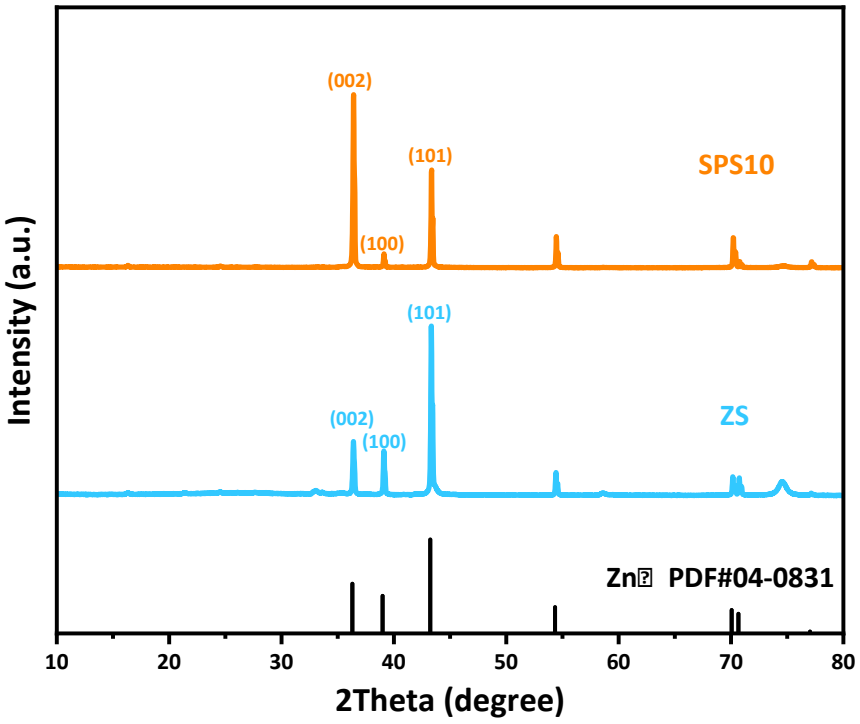

Figure S15. XRD patterns of electroplated Zn on stainless steel foils with a fixed capacity of 10 mAh cm^{-2} at a current density of 1 mA cm^{-2} in different electrolytes.

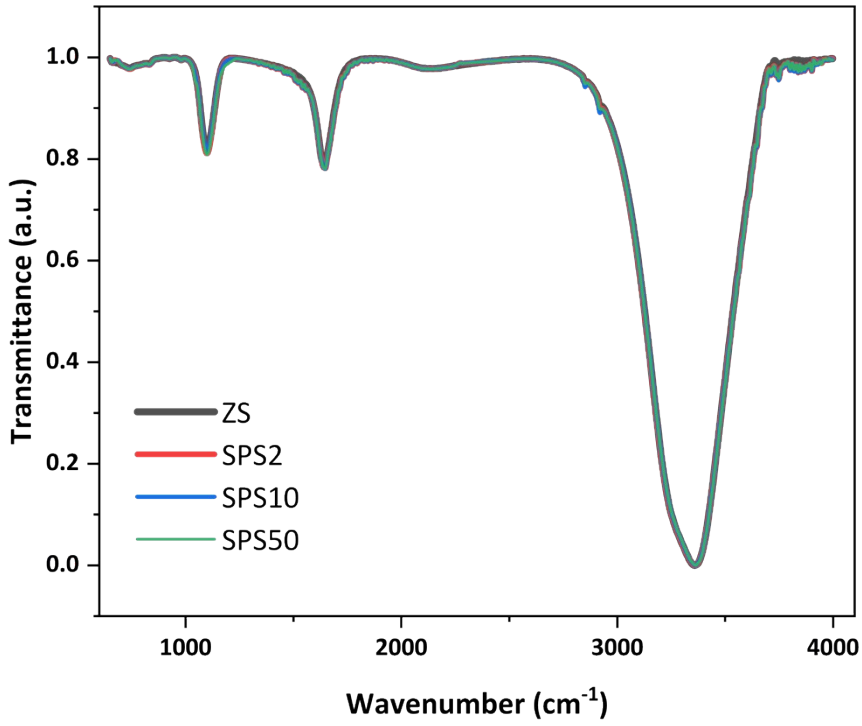

Figure S16. FTIR spectra of the $ZnSO_4$-based electrolytes with various concentrations of SPS additive.

The broad peak (2900–3700 cm^{-1}) can be attributed to the O–H stretching vibration of H_2O molecules, and the peak (1600–1700 cm^{-1}) comes from the bending vibration of H_2O molecules.[2] The peak at around 1100 cm^{-1} can be ascribed to the stretching vibration of SO_4^{2-}.[14] The peak position and peak intensity of the three peaks did not change with the addition of SPS, which further verifies that the solvation structure of the electrolyte has no change.

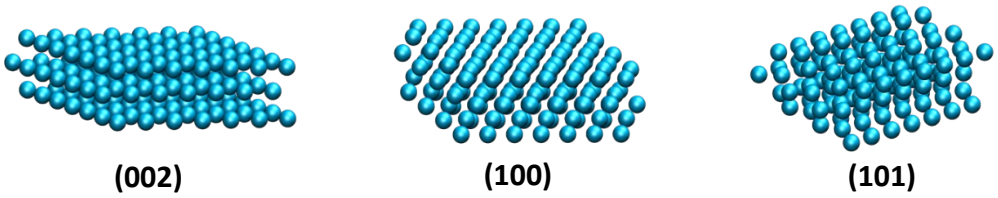

Figure S17. Slab models of Zn (002), Zn (100) and Zn (101).

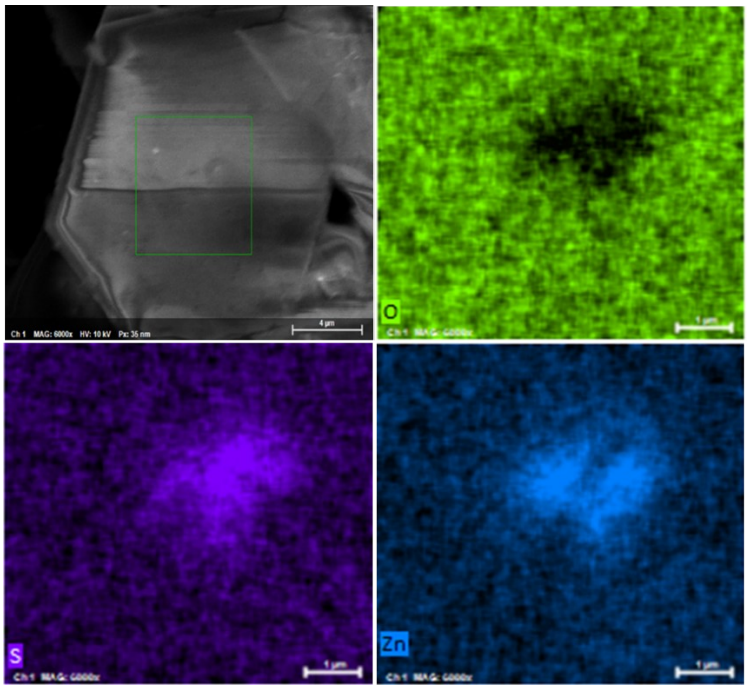

Figure S18. EDS mapping of Zn foil soaked in ZS electrolyte for 1 day, the green box represents the mapping area.

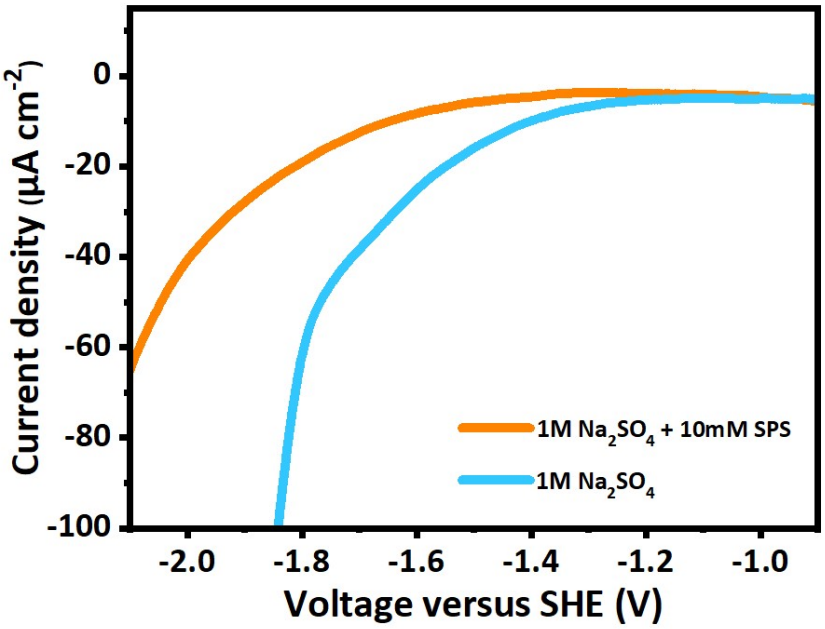

Figure S19. The LSV test plot of Na_2SO_4 electrolyte containing different concentrations of SPS.

It is worth mentioning that if zinc sulfate solution is used for LSV test, zinc ions will be preferentially precipitated during the test, and what we have measured is the precipitation potential of zinc ions, not hydrogen evolution potential. Thus, Na_2SO_4 solution was adopted to carry out the LSV test. The results in Figure S19 show that the hydrogen evolution potential in SPS10 electrolyte is lower than that in the other electrolyte, indicating that 10mM SPS additive can effectively improve the corrosion resistance of metal anode.

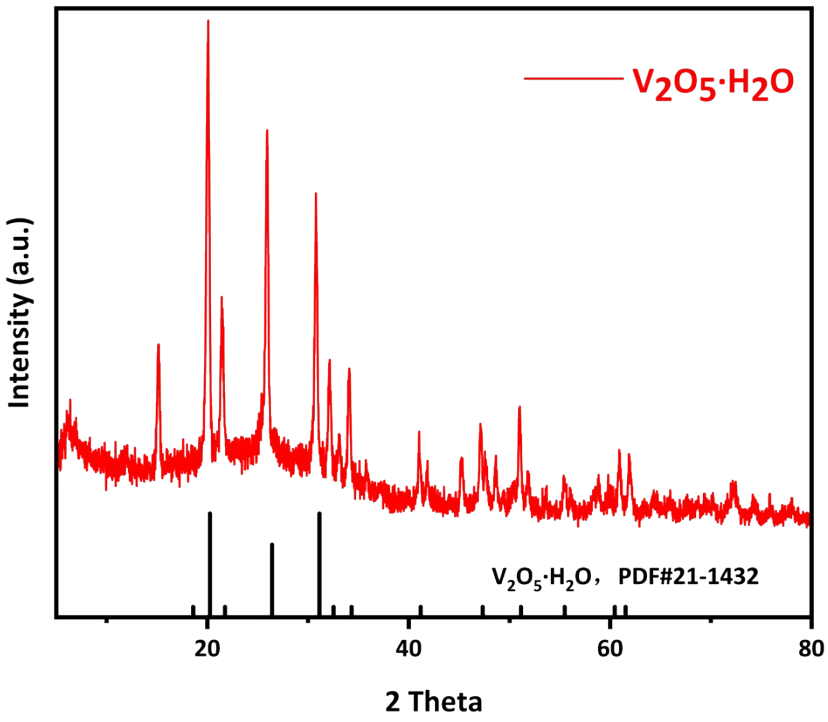

Figure S20. XRD pattern of the as-synthesized cathode material $V_2O_5 \cdot H_2O$.

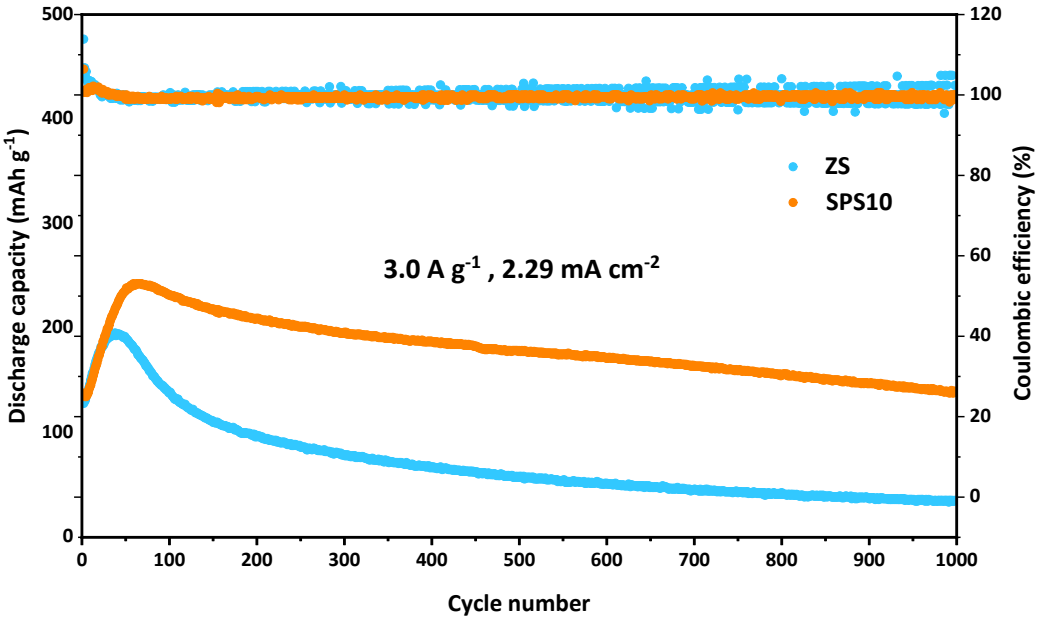

Figure S21. Long-term cycling performance of the Zn||VOH full cells at 3 A g^{-1} in different electrolytes.

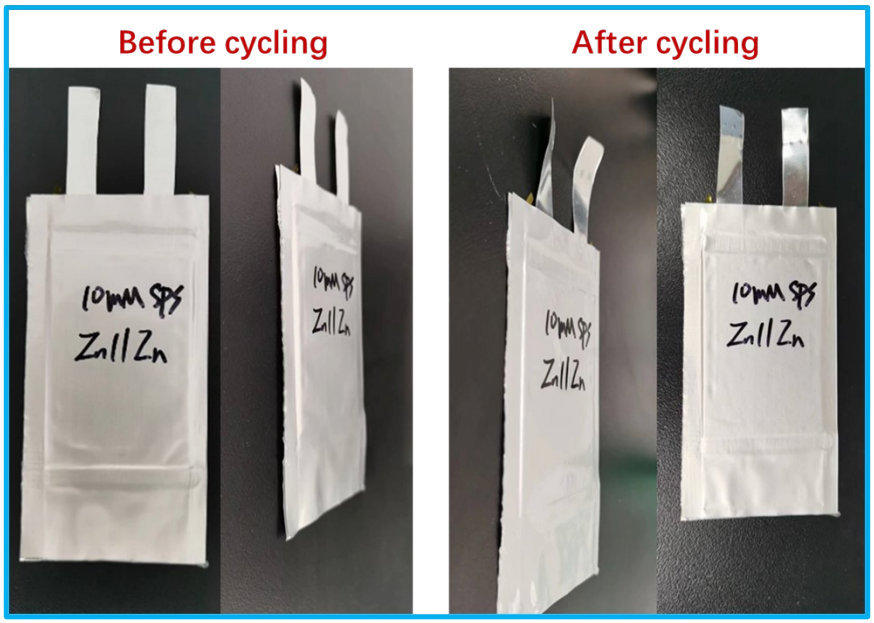

Figure S22. The digital photos of pristine/cycled pouch-type Zn||Zn symmetric cells with SPS10 electrolyte.

Table S1. Comparison of the cycling stability of Zn‖Zn symmetric cells assembled using different electrolyte additives.

No.	Modified electrolyte	Current density (mA cm^{-2})	Capacity density (mAh cm^{-2})	Lifespan (h)	Ref.
1	**1 M $ZnSO_4$ + 10mM SPS**	**1**	**1**	**4400**	**This work**
2	**1 M $ZnSO_4$ + 10mM SPS**	**5**	**5**	**870**	**This work**
3	1.3 M $ZnCl_2$/H_2O−DMSO (volume ratio of H_2O/DMSO = 4.3:1)	0.5	0.5	1000	[15]
4	20 mM $Zn(NO3)_2$ + aqueous 3M $Zn(OTF)_2$ electrolyte	0.5	0.5	1200	[16]
5	$Zn(TFSI)_2$-TFEP@MOF/H2O electrolyte	0.5	0.5	700	[17]
6	0.5 M $Zn(ClO_4)_2$ with 18 M $NaClO_4$	0.2	0.04	1200	[18]
7	1 M TC in 0.5 M ZnCl2	1	0.5	2145	[19]
8	1 M TC in 0.5 M ZnCl2	5	2.5	500	[19]
9	$ZnCl_2$: $Zn(OAc)_2$ = 10:6.	0.2	0.2	1200	[20]
10	1 M $ZnSO_4$ + 10mM Arg^+	0.5	0.5	500	[21]
11	1 M $ZnSO_4$ + 75 mM Na_4EDTA	2	2	450	[22]

12	1M $ZnSO_4$ +10 mM Glucose	1	1	2000	[23]
13	3 M $ZnSO_4$ + 68 vol% Ethylene glycol	0.5	0.5	2668	[24]
14	$Zn_3(PO_4)_2$ and ZnF_2 (ZCS)	2	4	1200	[25]
15	2 M $ZnSO_4$ + 0.5 vol% DME	2	2	380	[26]
16	1 M $ZnSO_4$ + 4 M EMImCl	1	1	500	[27]
17	$ZnSO_4$ + $La(NO_3)_3$	1	1	1200	[28]
18	$ZnSO_4$ + 5 vol% NMP	1	1	540	[29]
19	2M $ZnSO_4$ + 0.1M MSG	2	2	2200	[30]
20	$ZnSO_4$ + CH_3COONH_4	2	1	2400	[31]
21	$ZnSO_4$ + Sorbitol (SBT)	1	1	1000	[32]
22	$ZnSO_4$ + Sorbitol (SBT)	5	5	480	[32]
23	1 M $ZnSO_4$ + 1000 ppm Coconut diethanolamide	0.5	0.5	1580	[33]
24	1 M $ZnSO_4$ + 5% 1, 4-Dioxane (DX)	5	2.5	600	[34]

Table S2. The corrosion current and corrosion potential acquired by Tafel test in Figure 4d.

Parameter / Electrolyte	Corrosion current ($mA\ cm^{-2}$)	Corrosion potential (mV)
ZS	23	−16.8
SPS10	10	−12.6

Table S3. The relative content of elements obtained by EDS test in Figure S9.

Element	Mass Norm. [%]	Atom [%]
O	14.85	39.41
S	7.85	10.40
Zn	77.30	50.20
Total	100.00	100.00

Supplementary References

[1] Wang, H.; Bi, X.; Bai, Y.; Wu, C.; Gu, S.; Chen, S.; Wu, F.; Amine, K.; Lu, J. Open-Structured $V_2O_5 \cdot nH_2O$ Nanoflakes as Highly Reversible Cathode Material for Monovalent and Multivalent Intercalation Batteries. *Adv. Energy Mater.* 7(14), (2017).

[2] Ma, G.; Miao, L.; Dong, Y.; Yuan, W.; Nie, X.; Di, S.; Wang, Y.; Wang, L.; Zhang, N. Reshaping the Electrolyte Structure and Interface Chemistry for Stable Aqueous Zinc Batteries. *Energy Storage Mater.* 47, 203-210 (2022).

[3] Hafner, J. Ab-Initio Simulations of Materials Using VASP: Density-Functional Theory and Beyond. *J. Comput. Chem.* 29, 2044-2078 (2008).

[4] Kresse, G.; Furthmüller, J. Efficient Iterative Schemes for Ab Initio Total-Energy Calculations Using a Plane-Wave Basis Set. *Phys. Rev. B*, 54, 11169-11186 (1996).

[5] Perdew, J. P.; Chevary, J. A.; Vosko, S. H.; Jackson, K. A.; Pederson, M. R.; Singh, D. J.; Fiolhais, C. Atoms, Molecules, Solids, and Surfaces: Applications of the Generalized Gradient Approximation for Exchange and Correlation. *Phys. Rev. B*, 46, 6671-6687 (1992).

[6] Perdew, J. P.; Wang, Y. Accurate and Simple Analytic Representation of The Electron-Gas Correlation Energy. *Phys. Rev. B*, 45, 13244-13249 (1992).

[7] Perdew, J. P.; Burke, K.; Ernzerhof, M. Generalized Gradient Approximation Made Simple. *Phys. Rev. Lett.* 77, 3865-3868 (1996).

[8] Blöchl, P. E. Projector Augmented-Wave Method. *Phys. Rev. B*, 50, 17953-17979 (1994).

[9] Kresse G.; Joubert, D. From Ultrasoft Pseudopotentials to the Projector Augmented-Wave Method. *Phys. Rev. B*, 59, 1758-1775 (1999).

[10] Grimme, S.; Antony, J.; Ehrlich, S.; Krieg, H. A Consistent and Accurate Ab Initio Parametrization of Density Functional Dispersion Correction (DFT-D) for the 94 Elements H-Pu. *J. Chem. Phys.* 132, 154104 (2010).

[11] Humphrey, W.; Dalke, A.; Schulten, K. VMD: Visual Molecular Dynamics. *J.*

Mol. Graph. 14, 33-38 (1996).

[12] Hsin, J.; Arkhipov, A.; Yin, Y.; Stone, J. E.; Schulten, K. Using VMD: An Introductory Tutorial. *Curr. Protoc. Bioinformatics,* 24, 5.7.1-5.7.48 (2008).

[13] Monkhorst, H. J. & Pack, J. D. Special Points for Brillouin-Zone Integrations. *Phys. Rev. B.* 13, 5188–5192 (1976).

[14] Alemu, D.; Wei, H.; Hod, K.; Chu, C. Highly Conductive PEDOT: PSS Electrode by Simple Film Treatment with Methanol for ITO-free Polymer Solar Cells. *Energy Environ. Sci.* 5, 9662 (2012).

[15] Cao, L.; Li, D.; Hu, E.; Xu, J.; Deng, T.; Ma, L.; Wang, Y.; Yang, X.; Wang, C. Solvation Structure Design for Aqueous Zn Metal Batteries. *J. Am. Chem. Soc.* 142 (51), 21404-21409 (2020).

[16] Li, D.; Cao, L.; Deng, T.; Liu, S.; Wang, C. Design of a Solid Electrolyte Interphase for Aqueous Zn Batteries. *Angew. Chem. Int. Ed.* 60 (23), 13035-13041 (2021).

[17] Cao, L.; Li, D.; Deng, T.; Li, Q.; Wang, C. Hydrophobic Organic-Electrolyte-Protected Zinc Anodes for Aqueous Zinc Batteries. *Angew. Chem. Int. Ed.* 59 (43), 19292-19296 (2020).

[18] Zhu, Y.; Yin, J.; Zheng, X.; Emwas, A. H.; Lei, Y.; Mohammed, O. F.; Cui, Y.; Alshareef, H. N. Concentrated Dual-Cation Electrolyte Strategy for Aqueous Zinc-Ion Batteries. *Energy Environ. Sci.* 14 (8), 4463-4473 (2021).

[19] Yao, R.; Qian, L.; Sui, Y.; Zhao, G.; Guo, R.; Hu, S.; Liu, P.; Zhu, H.; Wang, F.; Zhi, C.; Yang, C. A Versatile Cation Additive Enabled Highly Reversible Zinc Metal Anode. *Adv. Energy Mater.* 12 (2), 2102780 (2021).

[20] Yang, M.; Zhu, J.; Bi, S.; Wang, R.; Niu, Z. A Binary Hydrate-Melt Electrolyte with Acetate-Oriented Cross-Linking Solvation Shells for Stable Zinc Anodes. *Adv. Mater.* 34 (18), 202201744 (2022).

[21] Chen, Z.; Chen, H.; Che, Y.; Cheng, L.; Zhang, H.; Chen, J.; Xie, F.; Wang, N.; Jin, Y.; Meng, H. Arginine Cations Inhibiting Charge Accumulation of Dendrites

and Boosting Zn Metal Reversibility in Aqueous Rechargeable Batteries. *ACS Sustain. Chem. Eng.* 9 (19), 6855-6863 (2021).

[22] Zhang, S.; Hao, J.; Luo, D.; Zhang, P.; Zhang, B.; Davey, K.; Lin, Z.; Qiao, S. Dual-Function Electrolyte Additive for Highly Reversible Zn Anode. *Adv. Energy Mater.* 11 (37), 2102010 (2021).

[23] Sun, P.; Ma, L.; Zhou, W.; Qiu, M.; Wang, Z.; Chao, D.; Mai, W. Simultaneous Regulation on Solvation Shell and Electrode Interface for Dendrite-Free Zn Ion Batteries Achieved by a Low-Cost Glucose Additive. *Angew. Chem. Int. Ed.* 60 (33), 18247-18255 (2021).

[24] Qin, R.; Wang, Y.; Zhang, M.; Wang, Y.; Ding, S.; Song, A.; Yi, H.; Yang, L.; Song, Y.; Cui, Y.; Liu, J.; Wang, Z.; Li, S.; Zhao, Q.; Pan, F. Tuning Zn^{2+} Coordination Environment to Suppress Dendrite Formation for High-Performance Zn-Ion Batteries. *Nano Energy* 80, 105478 (2021).

[25] Chu, Y.; Zhang, S.; Wu, S.; Hu, Z.; Cui, G.; Luo, J. In Situ Built Interphase with High Interface Energy and Fast Kinetics for High Performance Zn Metal Anodes. *Energy Environ. Sci.* 14 (6), 3609-3620 (2021).

[26] Cui, J.; Liu, X.; Xie, Y.; Wu, K.; Wang, Y.; Liu, Y.; Zhang, J.; Yi, J.; Xia, Y. Improved Electrochemical Reversibility of Zn Plating/Stripping: A Promising Approach to Suppress Water-Induced Issues Through the Formation of H-Bonding. *Mater. Today Energy* 18, 100563 (2020).

[27] Zhang, Q.; Ma, Y.; Lu, Y.; Zhou, X.; Lin, L.; Li, L.; Yan, Z.; Zhao, Q.; Zhang, K.; Chen, J. Designing Anion-Type Water-Free Zn^{2+} Solvation Structure for Robust Zn Metal Anode. *Angew. Chem. Int. Ed.* 60 (43), 23357-23364 (2021).

[28] Zhao, R.; Wang, H.; Du, H.; Yang, Y.; Gao, Z.; Qie, L.; Huang, Y. Lanthanum Nitrate as Aqueous Electrolyte Additive for Favourable Zinc Metal Electrodeposition. *Nat. Commun.* 13 (1), 3252 (2022).

[29] Li, T.; Lim, Y.; Li, X.; Luo, S.; Lin, C.; Fang, D.; Xia, S.; Wang, Y.; Yang, H. A Universal Additive Strategy to Reshape Electrolyte Solvation Structure toward

Reversible Zn Storage. *Adv. Energy Mater.* 12 (15), 2103231 (2022).

[30] Zhong, Y.; Cheng, Z.; Zhang, H.; Li, J.; Liu, D.; Liao, Y.; Meng, J.; Shen, Y.; Huang, Y. Monosodium Glutamate, an Effective Electrolyte Additive to Enhance Cycling Performance of Zn Anode in Aqueous Battery. *Nano Energy* 98, 107220 (2022).

[31] Lin, C.; Yang, X.; Xiong, P.; Lin, H.; He, L.; Yao, Q.; Wei, M.; Qian, Q.; Chen, Q.; Zeng, L. High-Rate, Large Capacity, and Long Life Dendrite-Free Zn Metal Anode Enabled by Trifunctional Electrolyte Additive with a Wide Temperature Range. *Adv. Sci.* 9 (21), 2201433 (2022).

[32] Qiu, M.; Sun, P.; Qin, A.; Cui, G.; Mai, W. Metal-Coordination Chemistry Guiding Preferred Crystallographic Orientation for Reversible Zinc Anode. *Energy Storage Mater.* 49, 463-470 (2022).

[33] Zhou, M.; Chen, H.; Chen, Z.; Hu, Z.; Wang, N.; Jin, Y.; Yu, X.; Meng, H. Nonionic Surfactant Coconut Diethanol Amide Inhibits the Growth of Zinc Dendrites for More Stable Zinc-Ion Batteries. *ACS Appl. Energy Mater.* 5 (6), 7590-7599 (2022).

[34] Feng, R.; Chi, X.; Qiu, Q.; Wu, J.; Huang, J.; Liu, J.; Liu, Y. Cyclic Ether-Water Hybrid Electrolyte-Guided Dendrite-Free Lamellar Zinc Deposition by Tuning the Solvation Structure for High-Performance Aqueous Zinc-Ion Batteries. *ACS Appl. Mater. Interfaces* 13 (34), 40638-40647 (2021).